Effect of thickness on the optical and electrical properties of ITO/Au/ITO sandwich structures.

Ka Kin Lam[1], Sheung Mei Ng[1], Hon Fai Wong[1], Linfeng Fei[1], Yukuai Liu[1], Ka Ho Chan[1], Hui Ye[2], Chi Wah Leung[1], Chee Leung Mak[1,]*

[1]Department of Applied Physics, The Hong Kong Polytechnic University, Hong Kong SAR, China

[2]State Key Laboratory of Modern Optical Instrumentation, Department of Optical Engineering, Zhejiang University, Hangzhou,310027, P. R. China

KEYWORDS: transparent conductive oxide, ITO/Au/ITO, asymmetric structure, electrical and optical properties, plasma frequency

ABSTRACT: Tin-doped indium oxide (ITO)/Au/ITO sandwich structures with varying top and bottom ITO film thicknesses were deposited by magnetron sputtering. The effects of varying thickness of the two ITO films on the structural, electrical and optical properties of the sandwich structures were investigated. X-ray diffraction (XRD) spectra showed that by inserting an ultrathin Au film, the average grain size of the top ITO layer was significantly increased, but not for the bottom one. The optical properties of the sandwich structures were measured by transmittance measurement and spectroscopic ellipsometry. In the symmetric structure where the top and the bottom ITO layers had the same thickness, we demonstrated that the crossover

wavelength can be changed from visible range (830 nm) to near infrared range (1490 nm) by increasing the top as well as bottom ITO thickness, corresponding to a plasmonic tuning ability of over 600 nm. The evaluation of this trilayer structure as plasmonic device was asserted based on three quality factors. Comparison of the performance of this trilayer structure with conventional materials was also discussed.

Introduction

Conventional noble metals such as gold (Au) and silver (Ag) have often been used in electronic and plasmonic applications, because of their high carrier concentrations, low resistivity and negative real permittivities over the visible to near-infrared (NIR) ranges. However, they also possess high optical losses due to inter-band electron scattering, making them unsuitable for plasmonic device applications in visible and/or near-infrared region. One of the alternatives is transparent conductive oxides (TCOs) which have been commonly used as transparent electrodes for optoelectronic devices. TCOs are usually transparency in visible range with relatively high conductivities, although their conductivities are not comparable with those of the pure noble metal. As a result, the plasmonic application of TCO is usually limited to wavelength between mid-infrared and near-infrared range. In order to take advantages of both noble metal and TCO and minimize their disadvantages, TCO/metal multilayer structure will be one of the possible solutions.

TCO/metal/TCO trilayer structure, a typical multilayer structure, has been widely studied in many fields such as electronics[1], plasmonic devices[2] and metamaterials.[3] This multilayer structure preserves the optical properties of the TCO, and at the same time possesses improved electrical properties by the insertion of the ultrathin metal layer. Indeed, this structure has the great applicability in plasmonic devices such as surface plasmon-polariton waveguides, localized

surface plasmon resonance-based devices, transformation optics devices and super lens.[4] General speaking, these applications are all related to the crossover wavelength of the structure, i.e. the wavelength that the real-part permittivity changes from positive to negative.[4] If the incident wavelength of electromagnetic wave is larger than the crossover wavelength, the optical properties of TCO materials will behave like metals. Most of the TCOs exhibit a crossover wavelength in the NIR region because of the relatively low carrier concentrations compared with metals. However, TCOs provide a great tunability in the electrical and optical properties through changing the processing conditions such as temperature,[5] deposition oxygen pressure[6] or insertion of a noble metal spacer[7]. So far, studies on thickness dependence properties of metal spacer[8-10] as well as top and bottom TCO layer[1, 11-12] and asymmetric material trilayers[13] have been reported. However, systemically study on the thickness dependence of the two sandwiched TCO layers on the optical and electrical properties of the trilayer structures has not been found. It is believed that this modification can also provide a possibility to tune not only the electrical and optical properties, but also the photonic or plasmonic properties of the trilayer structure.

In this paper, the thickness effect of the top and bottom ITO layers of symmetric ITO/Au/ITO sandwich structure (the top and bottom ITO thicknesses are the same and sandwiched with a ultrathin gold layer.) [14] on the electrical properties and optical properties of the structure from 400 nm to 2000 nm were investigated. Ellipsometric measurement was employed to extract the layer-by-layer optical properties and the corresponding thickness dependent effects. Gold, instead of other plasmonic noble metal such as silver, was chosen as the spacer layer because a thin layer of gold can improve the crystallinities of ITO that deposited on top of it, which has been previously demonstrated.[14] It is noticed that the difference in the crystallinities of top and bottom ITO layers will strongly affect the optical properties (the variation in optical properties

were represented in term of the permittivity) and electrical properties (such as carrier concentrations). Furthermore, the bottom and the top ITO in the trilayer were treated as two individual layers[14] and the sandwich layer modeled as a homogenous layer by the effective medium approximation (EMA) similar to $SiO_2/SiC/SiO_2$ trilayer structure.[15] The crossover wavelength of real-part of effective permittivity of composite films can be controlled in the range over 600 nm spanned from visible to NIR range. Therefore, the changes of the thickness can affect the overall optical properties of the trilayer structure. Finally, the performance of the structures was evaluated by comparing various surface plasmon polariton (SPP) parameters and plasmonic devices quality factors with some conventional plasmonic materials in order to estimate the potential application of this structure as plasmonic devices.

Experiment details

ITO/Au/ITO multilayer thin films were deposited by magnetron sputtering. The films were deposited on either Corning glass (Corning Eagle XG AMLCD glass) substrates for transmission measurements (due to their high transparency in the mid to long wavelength range) or SiO_2/Si substrates for electric measurements. All the substrates were first cleaned in acetone and then ethanol in an ultrasound bath for 10 minutes respectively and dried by a stream of nitrogen gas. After loading the substrates into the sputtering chamber, the chamber was evacuated to a base pressure of 2×10^{-6} torr. A flow of 30 sccm Ar was used to keep the deposition pressure maintained at 10^{-3} torr. The substrates were heated to $100^{o}C$ during the deposition process, as ITO films deposited at moderate temperature showed a lower resistivity compared with room temperature deposited one, bringing better electrical performance for the ITO thin films.[16] On the other hand, the deposition temperature was low enough to avoid the clustering of Au layer,

which ensured the deposited ultrathin gold layer to be uniform and continuous.[17] An 80W DC power was applied to the tin-doped indium oxide (In_2O_3/SnO_2 90/10 wt%, ITO thereafter) target and an 80W RF power was applied to the Au target (purity:99.99%) during deposition. During the deposition process, the substrates were rotated to obtain better thickness uniformity of the layers. All the three layers were deposited without breaking the vacuum to avoid any interface contamination. The thicknesses of the layers were controlled by varying the deposition time as decided according to the deposition rates obtained from thick calibration samples.

For a thorough characterization of the geometric influence of the trilayers on the performance of the samples, two sets of trilayer samples were investigated. 'Set A' samples consist of ITO (*t* nm)/Au (3 nm)/ITO (*t* nm) trilayers with geometrically symmetric structure (i.e. identical top and bottom ITO thicknesses) with different *t* values. This set of sample was used for investigating the influence of ITO/Au thickness ratio on the behavior of the structural as well as optical properties of the trilayer; 'Set B' samples, on the other hand, were used to explore the dependence of trilayer's structural properties as a function of Au layer position in the ITO/Au/ITO trilayers with invariant total thickness; this was done by depositing samples with varying bottom and top ITO thicknesses while keeping the *total* ITO thickness to be 40 nm (i.e. ITO (*x* nm)/Au (3 nm)/ITO [(40 – *x*) nm] trilayers, where *x* correspond to the top ITO thickness value. It is noticed that in both sets of the samples the Au layer thickness was kept constant (3 nm). The function of 'Set B' is to demonstrate the difference in the average grain size between top and bottom ITO layer by XRD measurements due to the insertion an ultrathin gold film. In summary, the thicknesses of 'Set A' and 'Set B' samples are listed in Table 1.

Table 1 The deposition time and the ITO (top and bottom) thickness of (a) Set A trilayers (t nm)/Au (3 nm)/ITO (t nm) and (b) Set B asymmetric trilayer structures. (40-t nm)/Au (3 nm)/ITO (t nm).

(a)

Sample Set A	Top ITO Deposition time (sec.)	Top ITO thickness (nm)*	Bottom ITO Deposition time (sec.)	Bottom ITO thickness (nm)*
S_a	100	11	100	11
S_b	200	22	200	22
S_c	300	33	300	33
S_d	400	44	400	44
S_e	500	55	500	55

*The thickness retrieved from the XRR measurement

(b)

Sample Set B	Top ITO Deposition time (sec.)	Top ITO thickness (nm)*	Bottom ITO Deposition time (sec.)	Bottom ITO thickness (nm)*
S_1	350	35	50	5
S_2	300	30	100	10
S_3	200	20	200	20
S_4	100	10	300	30
S_5	50	5	350	35

*The thickness retrieved from the XRR measurement

Structural properties of the trilayer structures were analyzed by X-ray diffractometry (XRD, Rigaku Smart Lab) and X-ray reflectivity (XRR) with Cu K_α radiation (λ = 0.1541 nm). Film thickness and the crystallinity of each film layer were investigated by transmission electron microscopy (TEM, Joel JEM-2100F). Electrical properties such as carrier concentration (n), Hall mobility (μ) and resistivity (ρ) were measured by a Keithley 6221 Current Source and a Keithley 2182A nanovoltmeter using the van der Pauw configuration, under a 0.5 T magnetic field. Ellipsometric parameters of the multilayers were measured by a GES-5E instrument (Semilab) between 400 and 2000 nm. Optical permittivity of the samples was obtained by fitting the ellipsometric angles ψ and Δ using the WinElli II software with suitable optical models. The optical transmittance was measured by PERKIN ELMER UV-Vis-NIR spectrometer in wavelength ranging from 400nm to 2000nm.

Results and Discussions

XRR was performed to measure the individual thicknesses of Set A trilayers, the results are shown in Figure 1. The measured XRR spectra were fitted in order to retrieve film thickness. The top and bottom ITO layer thicknesses were increased simultaneously from 11 nm to 55 nm while the middle Au layer was kept at about 3.0 nm i.e. the total thicknesses of the trilayers were varied in the range between 25 nm and 113 nm. Figure 1(a) and (b) show the XRD patterns of the Set A and Set B samples, respectively. In Figure 2(a), there is a sharp peak at about 35.1^o, corresponding to the ITO (400) peak that has been confirmed by the standard XRD pattern of powdered ITO. Another board peak at about 37.6^o, probably corresponding to the nano-sized gold layer is also observed.[18] The very board peak at ~23^o is arisen from the glass substrate. As both the top and bottom ITO film thickness becomes thicker, the ITO (400) peak gets sharper

(with the full width half-maximum (FWHM) changes from 0.59 to 0.31), indicating a larger average grain size is obtained. Our previous studies[14] showed that the top and bottom ITO films exhibit different levels of crystallinity and the insertion of Au spacer could improve the crystallinity of the top ITO layer.

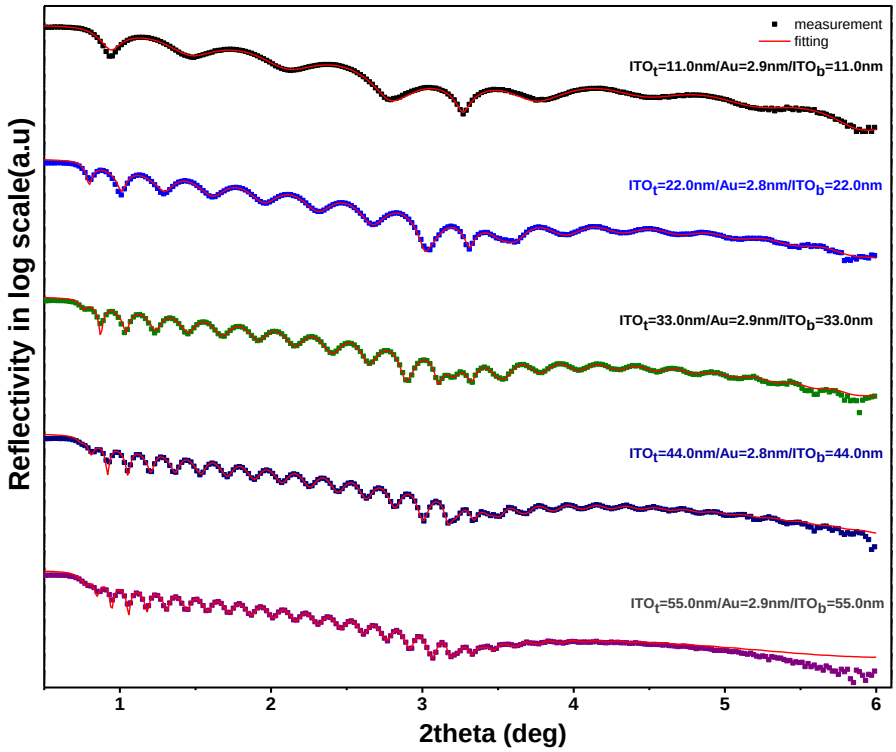

Figure 1.Measured (symbols) and fitted (solid lines) XRR pattern of ITO (t nm)/Au (2.9 nm)/ITO (t nm) trilayer films with different values of t.

To further investigate this hypothesis, set B samples (the asymmetric trilayer samples referenced by the ITO$_t$ (20 nm)/Au (3 nm)/ITO$_b$ (20 nm) symmetric geometry sample) with varying top and bottom ITO thickness while keeping the same total thickness of trilayer films (43nm) were fabricated. It can be observed that when the top and bottom ITO thickness is swapped (the comparison between S1 and S5 or S2 and S4), the XRD patterns as shown in Figure 2(b) behave differently. With increasing top ITO layer thickness, the observed ITO (400)

peak becomes sharper (FWHM = 0.33° for x = 35 sample S1), while the peak seems disappear on sample S5 with 35nm thick bottom ITO. On the other hand, all samples show a board peak at about 37°. By comparing Figure 2(a) and Figure 2(b), the originality of this peak arisen from the ultrathin gold layer can be confirmed.

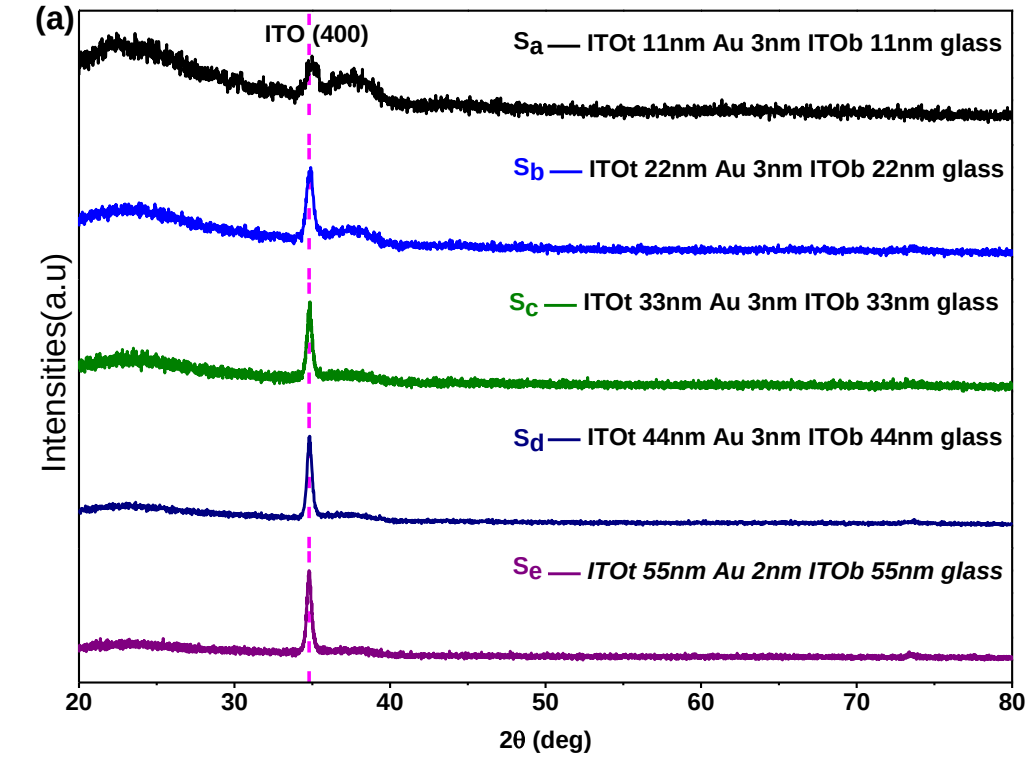
(a)
ITO (400)
Sa — ITOt 11nm Au 3nm ITOb 11nm glass
Sb — ITOt 22nm Au 3nm ITOb 22nm glass
Sc — ITOt 33nm Au 3nm ITOb 33nm glass
Sd — ITOt 44nm Au 3nm ITOb 44nm glass
Se — ITOt 55nm Au 2nm ITOb 55nm glass
Intensities(a.u)
20
30
40
50
60
70
80
2θ (deg)

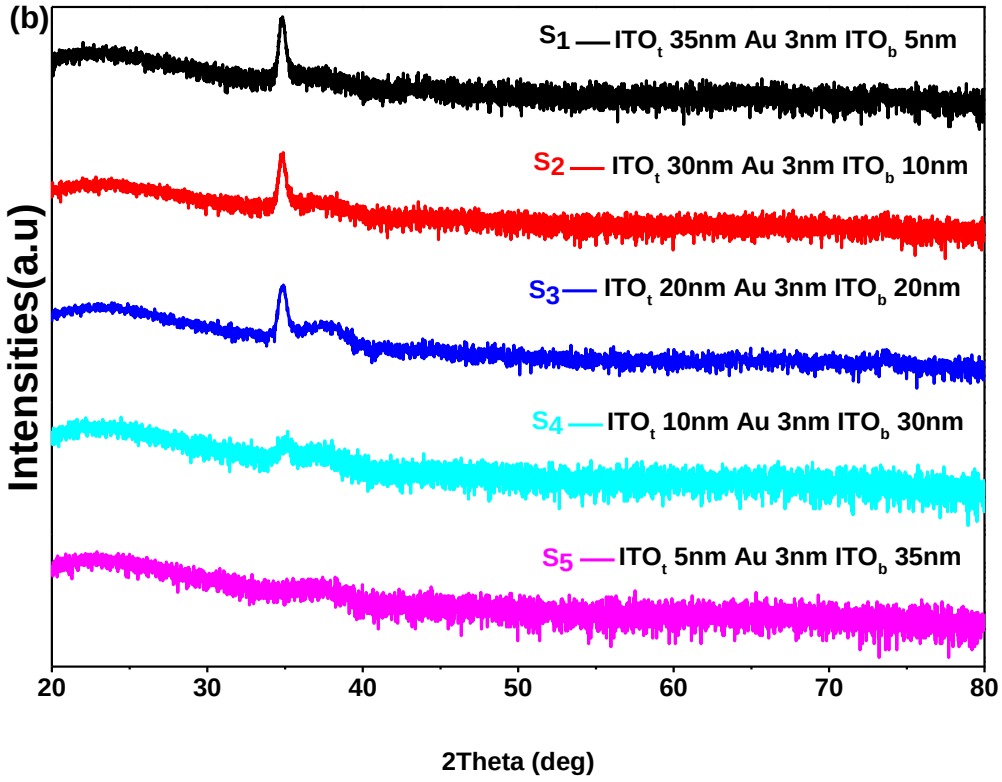
(b)
S1 — ITOt 35nm Au 3nm ITOb 5nm
S2 — ITOt 30nm Au 3nm ITOb 10nm
S3 — ITOt 20nm Au 3nm ITOb 20nm
S4 — ITOt 10nm Au 3nm ITOb 30nm
S5 — ITOt 5nm Au 3nm ITOb 35nm
Intensities(a.u)
20
30
40
50
60
70
80
2Theta (deg)

Figure 2 XRD patterns of Set A samples with values of thickness of each ITO layer (t nm) (a), and Set B samples as a function of the top ITO thickness (x nm) (b); bottom ITO thickness being (40 – x) nm

The average ITO grain size of the top ITO layer was estimated by the FWHM of the ITO (004) peak using the Scherrer's equation:

$$D = \frac{0.9\lambda}{\beta cos\theta} \quad (1)$$

where D is the average grain size, β is the FWHM of the peak and θ is the Bragg's diffraction angle. Figure 3 plots the effect of the ITO thickness on β of the (400) ITO peak in the symmetric trilayers. As expect, as ITO thickness increases, β gradually decreases and D gets larger for the top ITO layer (i.e. better crystallinity of the film is resulted). However, the bottom layers did not show any significant change in the FWHM values, which indicated that the increase in bottom layer thickness did not help much in improving the crystallinity of the ITO film directly grown on glass substrate. The result suggested that there is difference in the crystallinity of bottom and top ITO layers, and the Au spacer improves the crystallinity of the ITO film deposited on it.

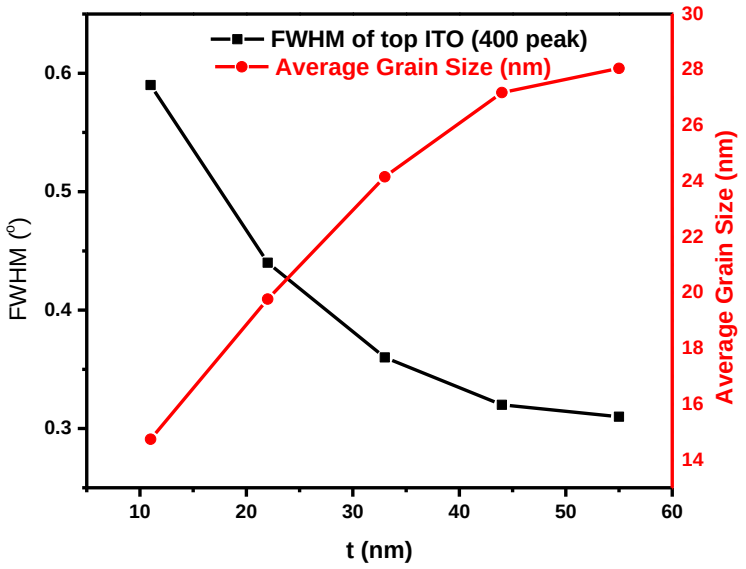

Figure 3 FWHM of (400) peak (squares) and top ITO layer average grain size (dots) for Set A samples as a function of t (c.f. Figure 2(a)). Lines are guides to the eye.

Cross-sectional TEM of the sample with $t = 20$ for both top and bottom ITO layers is shown in Figure 4(a). High uniformity in thickness is observed in all layers of the sandwich structure, probably due to the sample rotation process. Above all, the ultrathin gold layer is highly uniform and processes well-defined boundaries. The thicknesses obtained in the TEM micrographs matched well with those obtained in our XRR measurement as indicated in Table 1. Figure 4(b) shows the TEM selective area electron diffraction pattern on the top ITO layer of ITO (20 nm)/Au (3 nm)/ITO (20 nm) sample. Clear diffraction spots are obtained in the pattern, demonstrating the polycrystalline nature of the top ITO layer.

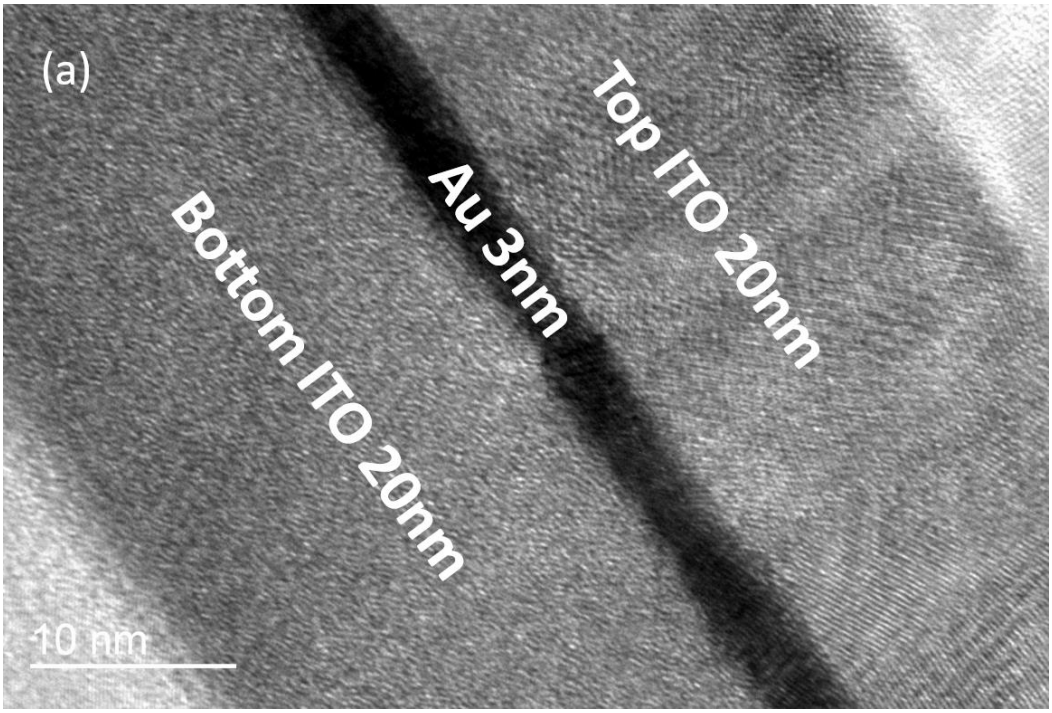

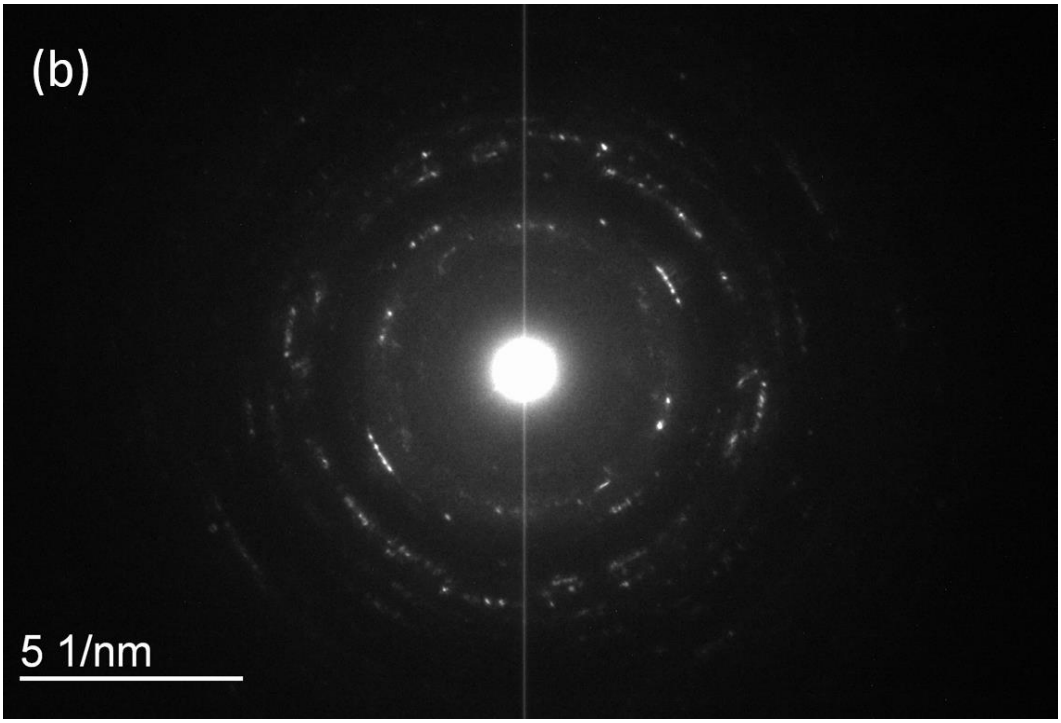

Figure 4 (a) Cross-sectional TEM of the ITO (20 nm)/Au (3 nm)/ITO (20 nm) sample. (b) Selected-area diffraction pattern of top ITO layer.

Figure 5 shows the results of electrical characterization of Set A trilayers. With same preparation conditions, we expect that the variation of the measured n, μ and ρ to be mainly arisen from the film thickness and differences in crystallinity. Comparing with 65nm pure ITO film on glass with carrier concentration in the range of $10^{19}/cm^3$, the measured n of the trilayers is two orders of magnitude higher, probably due to the carrier injection from the inserted Au layer.[19] As the ITO layer thickness increases, the carrier injection effect becomes less significant and the overall carrier concentration approaches that of pure ITO. On the other hand, the measured μ of the trilayers is smaller than that of pure ITO ($\approx 20\ cm^2V^{-1}s^{-1}$), because the carrier movement is severely affected by the interface scattering between Au and ITO layers.[20] When the ITO film thickness increases, the scattering effect becomes less significant and the value of μ approaches that of pure ITO.[7] In terms of resistivity, pure ITO film ($\approx 6.4\times10^{-3}\Omega cm$) is an order of magnitude larger than that of the trilayers prepared in this work.

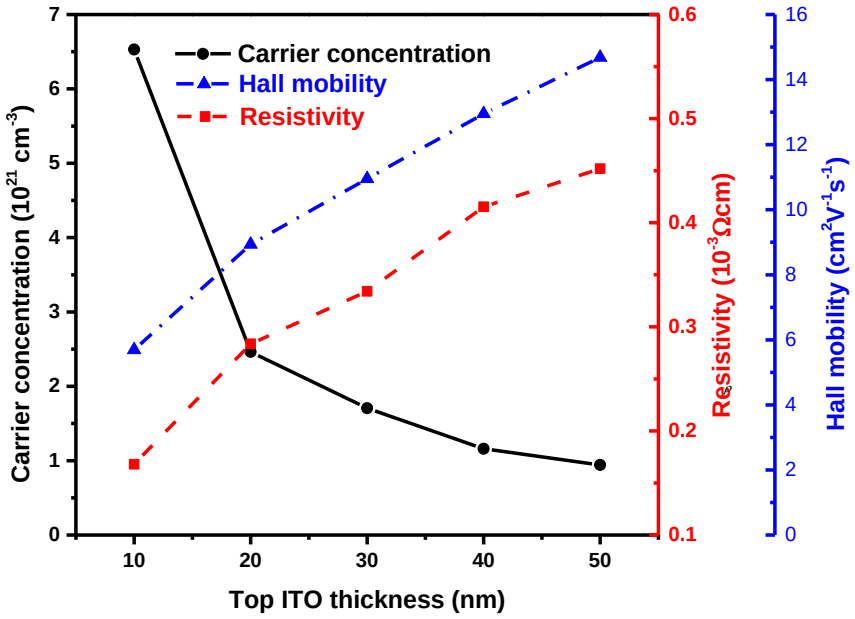

Figure 5 ITO layer thickness dependence of n(dots), μ (triangles) and ρ (squares) for Set A trilayers. Lines are guide to the eye.

As observed in Figure 5, an increase in ITO layer thickness for Set A samples is accompanied by an increase in μ. We believe that the increase in the grain size of the top ITO layer (Figure 3) is responsible for such observation. The larger grain size reduces the density of grain boundaries, thus the effect of boundary scattering is suppressed, resulting in an improvement of the charge mobility. [21]

Figure 6 shows the ellipsometric measurement between 400 nm and 2000 nm for Set A trilayer with ITO layer thickness of 22 nm. The dielectric functions of individual layers were determined using spectroscopic ellipsometric data with appropriate fitting models. It was reported that the trilayer with an ITO/Au/ITO layer structure could be described by simple Drude model with high accuracy without adding Cauchy or Lorentz components.[14] Since the current samples focus on

the variation of the ITO thickness, for a better evaluation in the optical properties of ITO layer, it is more suitable to add two Lorentz oscillator terms beyond the Drude model.[20]

$$\varepsilon = \varepsilon_\infty + \frac{{\omega_p}^2}{-\omega^2 + i\Gamma_D\omega} + \sum_{j=1}^{2} \frac{f_j {\omega_{oj}}^2}{\omega_{oj}^2 - \omega^2 + i\Gamma_j\omega} \quad (2)$$

$${\omega_p}^2 = \frac{n\,e^2}{\varepsilon_o m^*} \quad (3)$$

Here, ε_∞ is the high frequency permittivity, Γ_D is the Drude damping term. For the Lorentz oscillator, the f_j and Γ_j are the strength and damping constant of the Lorentz oscillator j. ω_{oj}^2 is the resonant angular frequency of the oscillator j which is related to the energy band gap of the material. ω_p is the plasma frequency of the material, the relation is given in Equation (3), which is related to the n and effective electron mass m^* of the material.

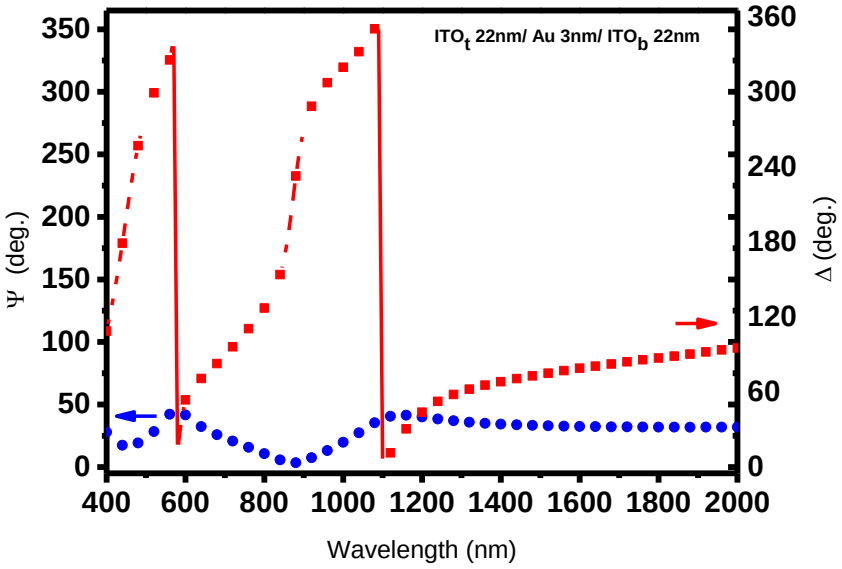

Figure 6 ψ and Δ of the ITO (22 nm)/Au (3 nm)/ITO (22 nm) sample measured by spectroscopic ellipsometry in the 400-2000 nm wavelength range.

Figure 7 (a) and (b) show the real (ε_r) and imaginary (ε_i) parts of permittivity of the bottom and top ITO layers retrieved from the ellipsometry measurement of Set A trilayers and fitted by the Drude-Lorentz model, respectively. ε_r is related to n (the refractive index) as well as the loss mechanism of conduction electron such as electron-electron interaction, electron-phonon interaction and grain boundary scattering. On the other hand, ε_i is responsible for the optical losses due to the plasma damping and free carrier absorption. Larger n leads to a stronger carrier absorption in the NIR range and contributes to a higher optical loss in long wavelengths. Therefore ε_i is generally higher in thinner sample, and the polycrystalline top ITO film shows little variation in ε_i in far NIR range as compared to the bottom ITO layer. [22]

Figure 7(c) plots the crossover wavelength λ_c (obtained from Figure 7(a)) of the upper ITO layers. It is noticed that λ_c shifts to smaller values as the top ITO layer thickness increases. However, as shown in Figure 7(b), no crossover is observed for the bottom ITO layer within our measured region. This can be explained by the difference of the crystallinity between the upper and bottom ITO layers. Compared to the amorphous nature of the bottom ITO layer, the top ITO layer has better crystallinity due to the gold spacer. Thus, we expect that the overall electrical behavior of trilayer might be dominated by the top ITO layer. As shown in Figure 5, we believe that the enhanced n and μ are related to the improvement of the crystallinity of the top ITO layer; while the increase in n is resulted from the blue shift of λ_c.

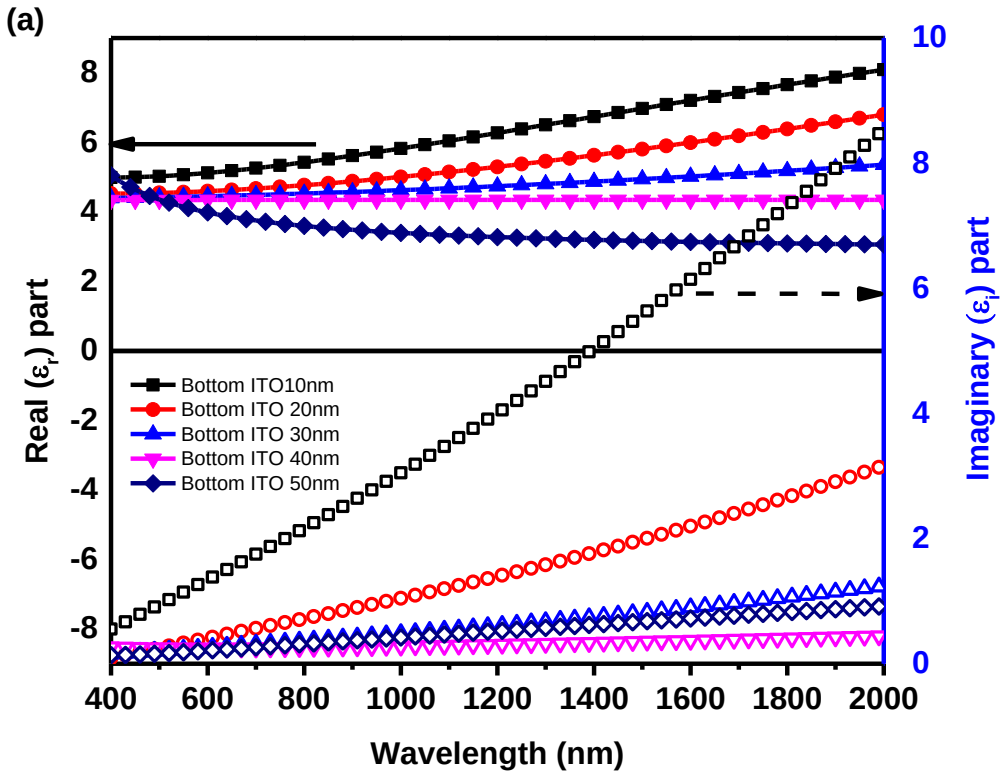
(a)
Real (ε_r) part
Imaginary (ε_i) part
Wavelength (nm)
Bottom ITO10nm
Bottom ITO 20nm
Bottom ITO 30nm
Bottom ITO 40nm
Bottom ITO 50nm

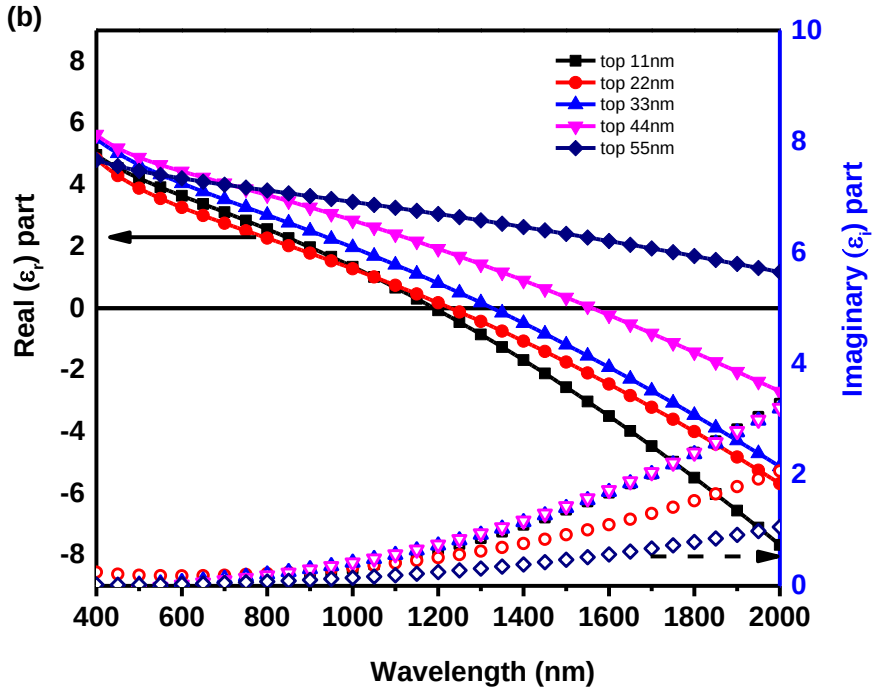
(b)
Real (ε_r) part
Imaginary (ε_i) part
Wavelength (nm)
top 11nm
top 22nm
top 33nm
top 44nm
top 55nm

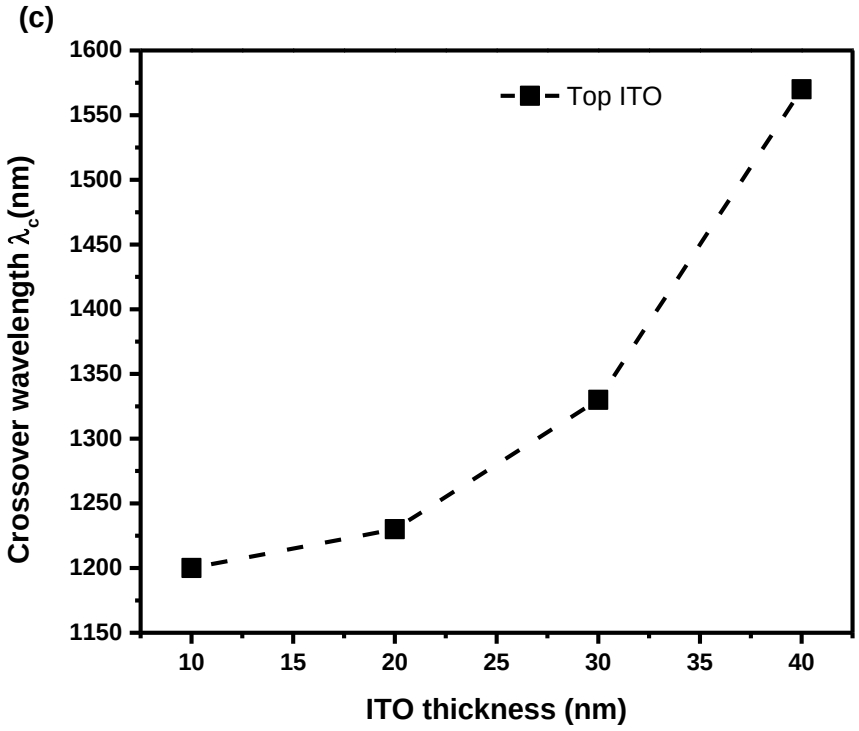

Figure 7 Real (solid symbols) and imaginary (open symbols) parts of permittivity against wavelength of (a) bottom ITO layer (b) top ITO layer in the Set A samples. (c) shows the crossover wavelength of the upper ITO layers in the Set A samples.

It is well known that the dispersion relation of TCO is related to the carrier concentration and the crystallinity of deposited films.[23] By inserting a gold layer, the crystallinity of the top ITO layer is improved, and the overall grain size of top ITO becomes larger than that of the bottom ITO layer. Furthermore, we expect that a smaller grain size results in more grain boundaries which decreases the free carrier concentration as free carriers will be trapped among the boundaries.[23] Therefore, we believe that the top ITO provides more free carriers than the bottom ITO. As shown in Figure 7(b), for the top ITO layer, the crossover wavelength shifts to shorter

wavelength as the film thickness decreases. At the same time, as the film thickness decreases, *n* increases as observed in the electrical measurements. According to Equation (3), ω_p^2 is directly proportional to *n*. Furthermore, we notice that ω_p is the reciprocal of the crossover wavelength. i.e. $\lambda c = \frac{2\pi c_p}{\omega_p}$ [24] where c_p corresponds to the velocity of plasma oscillation wave. Therefore, when ω_p increases due to an increase in *n*, it will result in the blue shift of λ_c. This trend is consistent with the results reported in the studies of thickness dependency of *n* in ITO films. [25-26] However, the amorphous bottom ITO layers show only positive ε_i over our measured spectral range. Therefore, the plasmon tuning ability by varying the thickness of the trilayer structure is strongly enhanced as compared with single ITO layer, which is mainly due to the existence of the top ITO layer which provides good tuning ability.

In order to investigate the optical properties of this metal-dielectric layered structure, which is a common type of hyperbolic metamaterial, an effective model was employed to estimate the collective effect contributed by the individual layers. Previous studies have demonstrated that effective medium approximation (EMA) is a reliable model in analyzing the optical properties of trilayer structure.[27,28] On the basis of this model, the trilayer structure was treated as a single optical anisotropic medium in both the parallel and perpendicular directions with two effective dielectric tensors ($\varepsilon_\perp$) and ($\varepsilon_{/\!/}^{-1}$), respectively, as defined in Eqts. (4) and (5). The derivation of the two tensors is based on Maxwell equations. For light incident on the vertical staked multilayer structures, the perpendicular direction is defined as the light propagated along three layers and the parallel direction related to the in-plane of the whole structure. Figure 8(a) shows the effective perpendicular permittivity of the trilayer structures, with λ_c varying from 830 nm to 1490 nm. From the figure, it is noticed that λ_c can be significantly modified within the NIR range by controlling the ITO thickness in the trilayer structure. This modification is based on the

difference of the dielectric properties among the two types of material. For metals, the abundance of free electrons yields a large plasma frequency, and the real permittivity of metal quickly becoming negative in the UV and visible spectral range.[4] Meanwhile, the low carrier density of ITO means that its real permittivity only crosses the zero (from positive to negative) within the NIR wavelength. Our results demonstrated that the variation of the ITO thickness and the insertion of a 3-nm Au spacer are capable of tuning the plasmonic behavior of the trilayer structure. Figure 8(b) shows the variation of the obtained λ_c as a function of the ITO thickness. It is noticed that λ_c increases linearly with the ITO thickness. As the EMA treats the whole trilayer as a homogenous system, the overall performance of the sample is of more important. With increasing ITO thickness, the film properties are dominated by the ITO layers and the contribution of Au spacer is suppressed. This makes the samples less metallic-like and causing the shift in the plasma frequency.

$$\varepsilon_{\perp} = \frac{1}{d_{ITO_{top}} + d_{Au} + d_{ITO_{bottom}}} (\varepsilon_{ITO_{top}} d_{ITO_{top}} + \varepsilon_{Au} d_{Au} + \varepsilon_{ITO_{bottom}} d_{ITO_{bottom}}) \quad (4)$$

$$\varepsilon_{/\!/}^{-1} = \frac{1}{d_{ITO_{top}} + d_{Au} + d_{ITO_{bottom}}} \left(\frac{d_{ITO_{top}}}{\varepsilon_{ITO_{top}}} + \frac{d_{Au}}{\varepsilon_{Au}} + \frac{d_{ITO_{bottom}}}{\varepsilon_{ITO_{bottom}}}\right) \quad (5)$$

In order to show the validity of EMA in modeling the dielectric properties of our trilayer structure, the simulated transmittance spectra of the trilayer samples (set A) of different ITO layer thicknesses obtained from the model were compared to the measured spectra. The measured transmittance spectra of the samples in Figure 9(a) are larger than 60% in the visible range (400 nm-700 nm), indicating that the trilayers preserve a high transparency even with an inserted gold layer. The maximum point observed in the transmittance curves is implying the

sharp interfaces and uniform thickness. The transmittance drop at longer wavelengths is due to the free carrier absorptions which is a typical observation in TCO.[29]

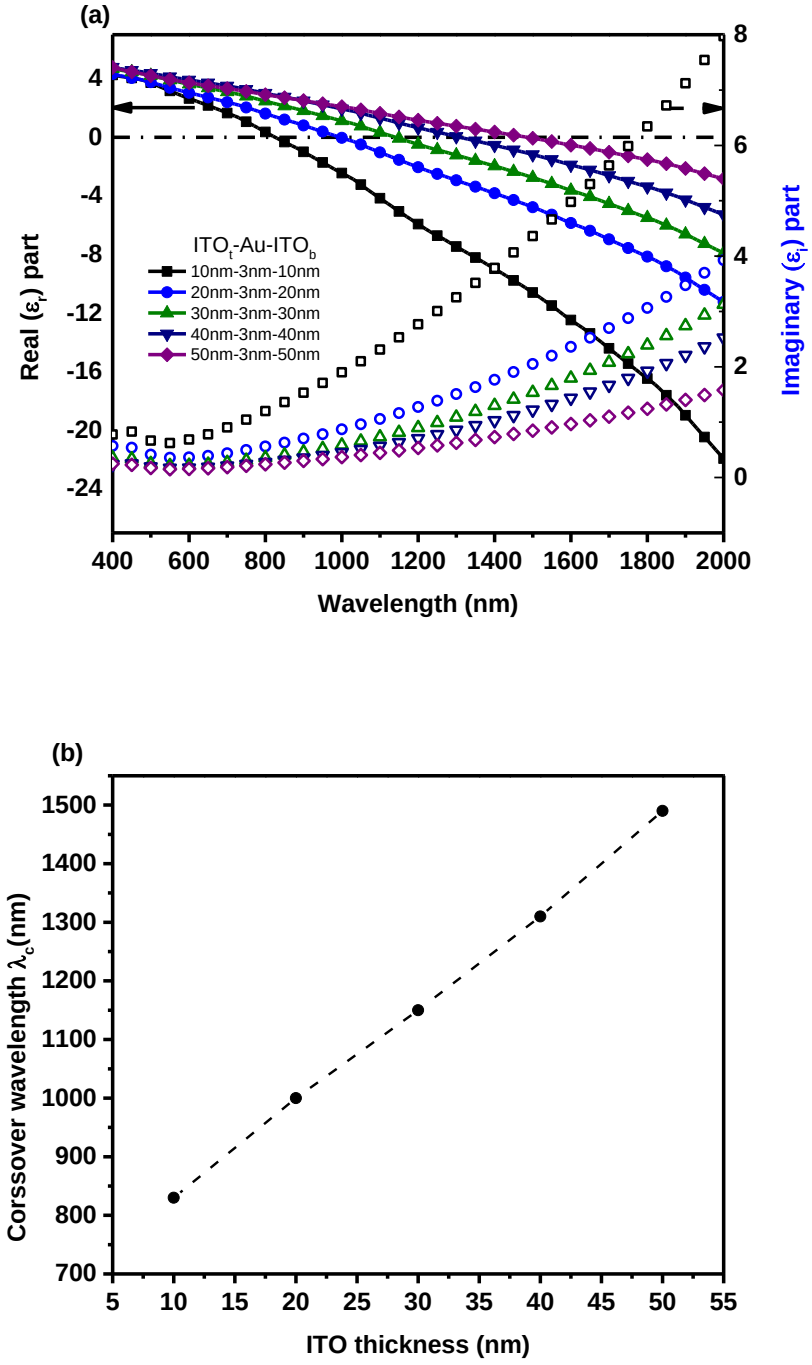

Figure 8 (a) Real part $\varepsilon_{\perp,r}$ (solid symbols) and imaginary part $\varepsilon_{\perp,i}$ (open symbols) of $\varepsilon_{\perp}$ for Set A trilayer samples as calculated by effective medium approximation. (b) λ_c as function of t in Set A samples.

Figure 9(b) plots the simulated transmittance of Set A trilayers using the EMA model, and the detail modeling is reported in the supplementary information. In the model, the initial parameters were obtained from the ellipsometric measurements. The refractive indices and extinction coefficients of various layers were calculated using the EMA as reported.[14, 28] The trilayer structures were treated as homogeneous layers with effective permittivity tensor $\varepsilon_{\perp}$ and $\varepsilon_{/\!/}^{-1}$[14] Comparing Figure 9(a) with Figure 9(b), we notice a reasonable match between experimental spectra and the simulated transmittance, particularly over the infrared region. Thus, we believe that the EMA model is a suitable model to describe the optical properties of the trilayer structure. Figure 9(c) is the result of simulated transmittance using the ellipsometry measurement result of the trilayer structure instead of using the EMA. The calculated result also shows similar trend among the EMA and experiment spectra. It is proven that an effective medium is a reliable means to reflect the optical properties of multilayer structures.

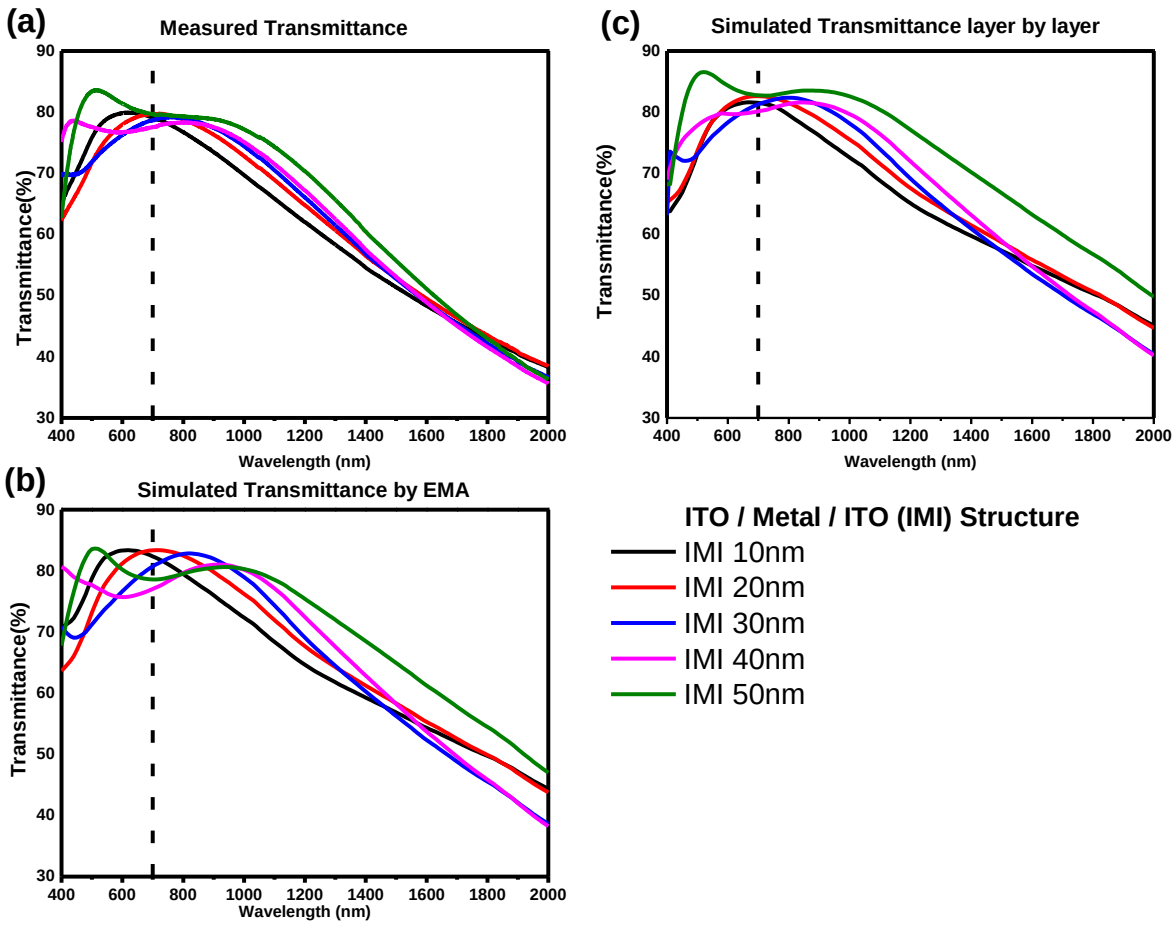

Figure 9 (a) Spectral transmittance of Set A trilayers with varying ITO thickness. (b) Simulated transmittance by effective media approximation. (c) Simulated transmittance of ITO/Au/ITO trilayer structure from ellipsometry results of the trilayer structure. (The left side of dashed line refer to visible wavelength range.)

Next, we consider the application potential of the ITO/Au/ITO structures. TCO thin films have been demonstrated to be applied as localized surface plasmon resonance (LSPR) device, surface plasmon-polariton (SPP) waveguides and transformation optics (TO).[4] The effectiveness of our trilayer structures for such plasmonic applications has been evaluated using the corresponding quality factors (Q_{LSPR}, Q_{SPP}, Q_{TO}) as defined in equations (6), (7) and (8). These quality factors of the trilayer structure were calculated from the complex effective permittivity $\varepsilon_{\perp}$ ($= \varepsilon'_{\perp} + i\varepsilon''_{\perp}$)

as defined in equation (4). From the Maxwell's equation $\varepsilon'_{\perp}$ indicates the field distribution in the material and the optical loss is quantified by $\varepsilon''_{\perp}$. Therefore, the quality factor should take both factors into consideration.

$$Q_{LSPR}(\omega) = \frac{-\varepsilon'_{\perp}(\omega)}{\varepsilon''_{\perp}(\omega)} \tag{6}$$

$$Q_{SSP}(\omega) = \frac{\varepsilon'_{\perp}(\omega) + \varepsilon'_{d}(\omega)}{\varepsilon'_{\perp}(\omega)\varepsilon'_{d}(\omega)} \frac{\varepsilon'_{\perp}(\omega)^2}{\varepsilon''_{\perp}(\omega)} \tag{7}$$

$$Q_{TO}(\omega) = \frac{1}{\varepsilon''_{\perp}(\omega)} \ (-\varepsilon'_{\perp} \sim \varepsilon_d \sim 1) \tag{8}$$

Figure 10 shows the variation of Q_{LSPR} as a function of wavelength for different trilayers. The profiles show that the ITO thickness in the trilayers has significant impact on Q_{LSPR} as well as the operation wavelengths. It should be noted that the curve is only available in the range $Q_{LSPR}>0$, as the incident field will be enhanced under such a situation. The result shows that a change in top and bottom ITO thickness in the trilayer not only control the spectral range of the LSPR device, but also can enhance the local field by a maximum factor of 2.5 to 3.0 depending on the thickness of ITO layer.

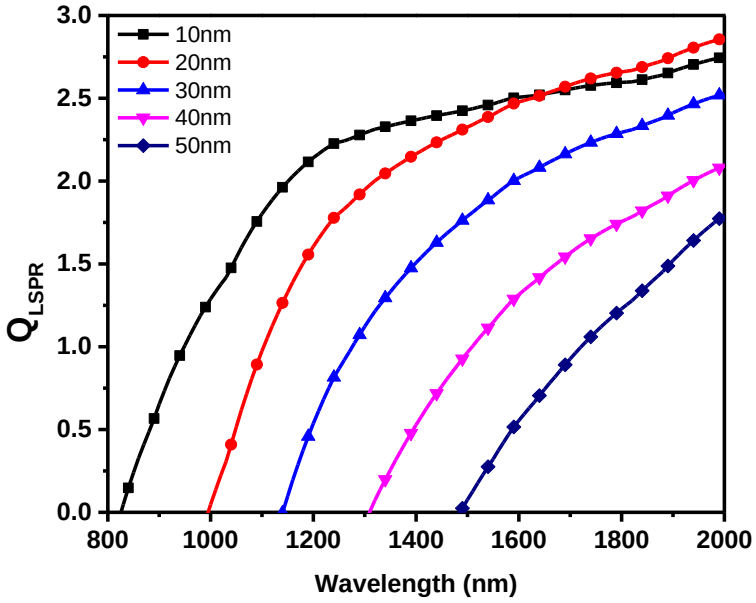

Figure 10 Q_{LSPR} variation with wavelength for Set A trilayers

A comprehensive comparison of the plasmonic figure of merits with the trilayer structures, pure ITO and, noble metals are listed in Table 2. The results not only indicate which structure has better performance in device application, but also determine which spectral wavelength has the best performance.[4] The advantages of using the ITO/Au/ITO trilayers instead of pure material in various plasmonic devices application are due to their high tunability of the operating plasmonic wavelength. Table 2 lists out the comparison of the quality factors of conventional noble metal (Au and Ag), TCO (ITO) and the trilayer structure for different plasmonic devices. The table reports the optimal wavelengths and the corresponding quality factors on device application. In the table, the corresponding quality factors at 1.5 μm are also reported.[4] This special reported wavelength is related to the nanophotonic applications. Although the quality

factors of IAI structure are not comparable to those of the pure metal, their overall performance is still better than the performance of pure ITO.

Table 2 Comparision of quality factors of three different plasmonic dervices with different materials. The quality factorse of 1.5 μm indicate the nanophotonic applications. (IAI structure data ends at 2 μm) [4]

Material	LSPR&SPR		SPP		TO Devices
	Maximum Q_{LSPR} (λ)	Q_{LSPR} (1.5 μm)	Maximum Q_{SPP} (λ)	Q_{SPP} (1.5 μm)	Q_{TO} (λ)
Ag	392 (1.08 μm)	39.3	23413 (1.08 μm)	4530	1.82 (326 nm)
Au	16.66 (0.89 μm)	10.63	1410 (1.94 μm)	1140	0.29 (207 nm)
ITO	2.72 (2.3 μm)	N/A	16 (2.3 μm)	N/A	1.54 (1.69 μm)
ITO/Au/ITO (10nm/3nm/10nm)	4.73 (1.34 μm)	4.61	96.0 (2 μm)	53.14	1.21 (0.66 μm)
ITO/Au/ITO (20nm/3nm/20nm)	2.56 (2 μm)	1.30	30.7 (2 μm)	13.28	0.93 (0.95 μm)
ITO/Au/ITO (30nm/3nm/30nm)	2.61 (2 μm)	2.39	44.9 (0.54 μm)	6.51	0.51 (1.36 μm)
ITO/Au/ITO (40nm/3nm/40nm)	1.87 (2 μm)	0.36	65.5 (0.52 μm)	0.14	0.56 (1.36 μm)
ITO/Au/ITO (50nm/3nm/50nm)	1.36 (2 μm)	0.09	173.8 (0.54 μm)	0.008	0.62 (1.37 μm)

Regarding SPP systems, the surface plasmon can be coupled with light strongly. This enhances the light-matter interactions, forming a surface plasmon-polariton waveguides to propagate the wave along the interface.[30] The trilayer can be regarded as a homogeneous medium, with the

surface plasmon propagating at the interface between the trilayer thin film and the silicon dioxide dielectric. In Equation (7) ε_d is the dielectric permittivity of the dielectric; here ε_d is taken as 2.37 for silicon dioxide and is set constant over the spectral range measured.

The SPP profile can be characterized by parameters such as the propagation length δ_{Prop} (distance of which the SPP intensity drops to 1/e of the original value as shown in Equation (9)), penetration lengths δ_{conf} (the penetration distance inside the material as shown in Equation (10)) and the SPP wavelength λ_{SPP} (Equation (11)).[31] In these equations ε_m' and ε_m'' are the real and imaginary parts of permittivity of the metal layer ε_m, which is the perpendicular effective tensor $\varepsilon_\perp$ of the trilayer film in our case. λ_0 is the wavelength of free space. [31]

$$\delta_{Prop} = \lambda_0 \frac{\varepsilon_m'}{2\pi\varepsilon_m''}\left(\frac{1+\varepsilon_m'}{\varepsilon_m''}\right)^{3/2} \tag{9}$$

$$\delta_{conf} = \frac{\lambda_0}{2\pi}\left|\frac{1+\varepsilon_m'}{\left(\varepsilon_m''\right)^2}\right|^{1/2} \tag{10}$$

$$\lambda_{SPP} = \frac{2\pi}{k_{SPP}'} = \lambda_0\sqrt{\frac{\varepsilon_d'+\varepsilon_m'}{\varepsilon_d'\,\varepsilon_m'}} \tag{11}$$

The profile of SPP properties is plotted in Figure 11. In the NIR range, the SPP generally has longer propagation length as the wavelength of incident light increases. For the trilayer thickness increases, the maximum propagation length decreases and approaches to the value as pure ITO film.

The penetration length determines the degree of confinement of the SPP at the metallic layer and is a measure of the compactness of the SPP behaviour. With increasing wavelength, the penetration length approaches to a constant value. The value decreases as the trilayer thickness

decreases, which means that the reduction in thickness can impose a high localization of the SPP. Figure 11(c) shows λ_{SPP} of the dielectric-trilayer interface, and the propagation wavelength is greater than the SPP wavelength in all spectral range. Therefore, it is possible to bring the trilayer into real application.[31]

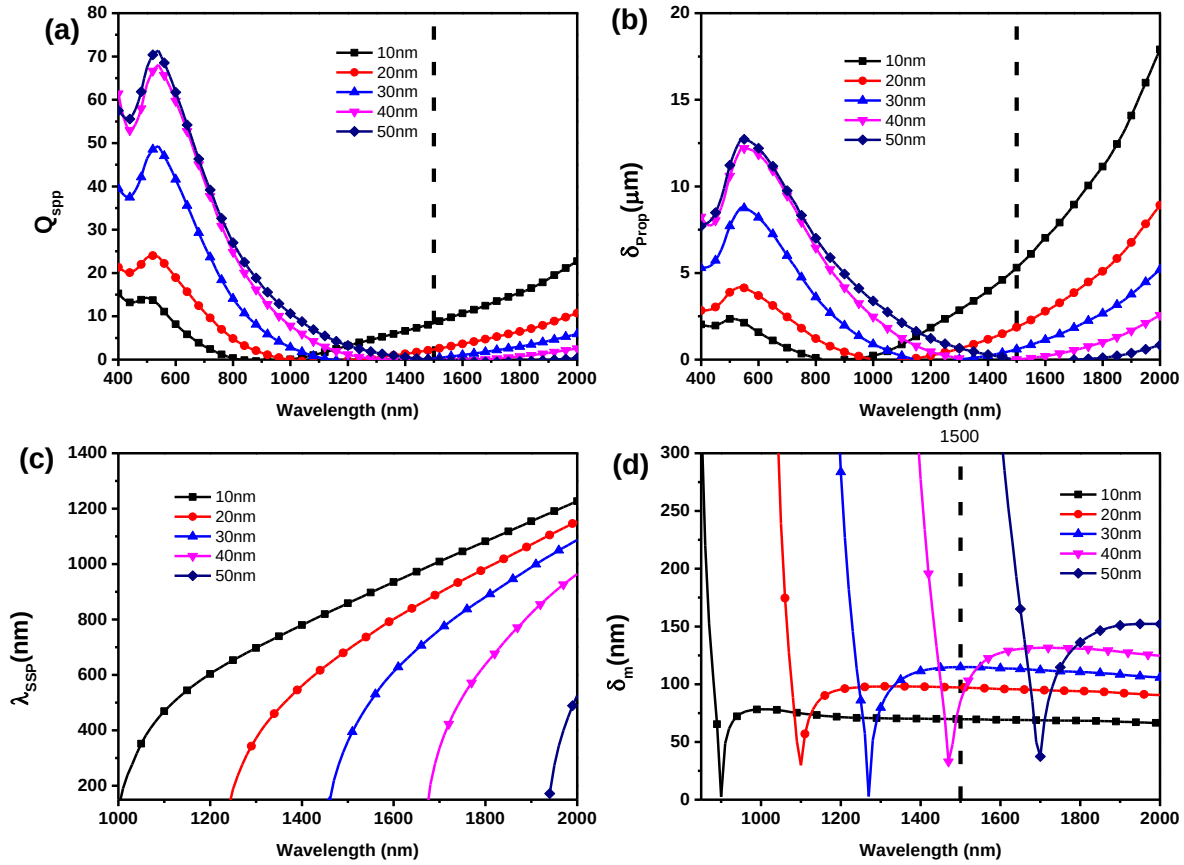

Figure 11 Spectral profile of SPP between silicon substrate and thin film interface for Set A trilayers: (a) quality factors Q_{SPP}, (b) propagation length δ_{prop}, (c)) SPP wavelength λ_{SPP} and (d) degree of confinement δ_{conf}.

Conclusion

ITO/Au/ITO sandwiched films with different ITO thickness and position of gold spacer layer were deposited on glass substrate by magnetron sputtering. The electrical and optical properties

can be manipulated by keeping the same structure and varying the top and bottom ITO layer. The plasmonic properties are highly dependent on the relative thickness between ITO and Au in the sandwich structure. The performance of potential application in the plasmonic device had also been evaluated from visible to NIR range.

ASSOCIATED CONTENT

Corresponding Author

*C.L.M.: e-mail, apaclmak@polyu.edu.hk; phone, (852)2766 5667; fax, (852)23337629.

ACKNOWLEDGMENTS

The First Author Ka Kin Lam was supported by The Hong Kong Polytechnic University (Grant G-SB0G).

Supporting Information

The supporting information is including the additional measurements of structural properties of trilayer structures (for example the omega scan of top ITO film and the thickness confirmation of asymmetric trilayer structure which done by XRR) to support the deduction in the article. Also, including the theory background of simulated transmittance using EMA and evaluation of the EMA applicability.

REFERENCE

1. Guillén, C.; Herrero, J., TCO/Metal/TCO Structures for Energy and Flexible Electronics. *Thin Solid Films* **2011,** *520* (1), 1-17.

2. Kiba, T.; Yanome, K.; Kawamura, M.; Abe, Y.; Kim, K. H.; Takayama, J.; Murayama, A., Emission Enhancement in Indium Zinc Oxide(IZO)/Ag/IZO Sandwiched Structure Due to Surface Plasmon Resonance of Thin Ag Film. *Applied Surface Science* **2016,** *389*, 906-910.
3. Tumkur, T.; Zhu, G.; Black, P.; Barnakov, Y. A.; Bonner, C. E.; Noginov, M. A., Control of Spontaneous Emission in a Volume of Functionalized Hyperbolic Metamaterial. *Applied Physics Letters* **2011,** *99* (15).
4. West, P. R.; Ishii, S.; Naik, G. V.; Emani, N. K.; Shalaev, V. M.; Boltasseva, A., Searching for Better Plasmonic Materials. *Laser & Photonics Reviews* **2010,** *4* (6), 795-808.
5. Kim, J. H.; Ahn, B. D.; Lee, C. H.; Jeon, K. A.; Kang, H. S.; Kim, G. H.; Lee, S. Y., Enhancement in Electrical and Optical Properties of Indium Tin Oxide Thin Films Grown Using a Pulsed Laser Deposition at Room Temperature by Two-Step Process. *Thin Solid Films* **2007,** *515* (7-8), 3580-3583.
6. Cui, H.-N.; Teixeira, V.; Meng, L.-J.; Martins, R.; Fortunato, E., Influence of Oxygen/Argon Pressure Ratio on the Morphology, Optical and Electrical Properties of ITO Thin Films Deposited at Room Temperature. *Vacuum* **2008,** *82* (12), 1507-1511.
7. Kim, Y. S.; Park, J. H.; Choi, D. H.; Jang, H. S.; Lee, J. H.; Park, H. J.; Choi, J. I.; Ju, D. H.; Lee, J. Y.; Kim, D., ITO/Au/ITO Multilayer Thin Films for Transparent Conducting Electrode Applications. *Applied Surface Science* **2007,** *254* (5), 1524-1527.
8. Park, H.-K.; Kang, J.-W.; Na, S.-I.; Kim, D.-Y.; Kim, H.-K., Characteristics of Indium-Free GZO/Ag/GZO and AZO/Ag/AZO Multilayer Electrode Grown by Dual Target DC Sputtering at Room Temperature for Low-Cost Organic Photovoltaics. *Solar Energy Materials and Solar Cells* **2009,** *93* (11), 1994-2002.
9. Girtan, M., Comparison of ITO/Metal/ITO and ZnO/Metal/ZnO Characteristics as Transparent Electrodes for Third Generation Solar Cells. *Solar Energy Materials and Solar Cells* **2012,** *100*, 153-161.
10. Sibin, K. P.; Srinivas, G.; Shashikala, H. D.; Dey, A.; Sridhara, N.; Kumar Sharma, A.; Barshilia, H. C., Highly Transparent and Conducting ITO/Ag/ITO Multilayer Thin Films on Fep Substrates for Flexible Electronics Applications. *Solar Energy Materials and Solar Cells* **2017,** *172*, 277-284.
11. Yu, S.; Zhang, W.; Li, L.; Xu, D.; Dong, H.; Jin, Y., Optimization of SnO_2/Ag/SnO_2 Tri-Layer Films as Transparent Composite Electrode with High Figure of Merit. *Thin Solid Films* **2014,** *552*, 150-154.
12. Vedraine, S.; El Hajj, A.; Torchio, P.; Lucas, B., Optimized Ito-Free Tri-Layer Electrode for Organic Solar Cells. *Organic Electronics* **2013,** *14* (4), 1122-1129.
13. Lee, S.-M.; Koo, H.-W.; Kim, T.-W.; Kim, H.-K., Asymmetric ITO/Ag/ZTO and ZTO/Ag/ITO Anodes Prepared by Roll-to-Roll Sputtering for Flexible Organic Light-Emitting Diodes. *Surface and Coatings Technology* **2018,** *343*, 115-120.
14. Fang, X.; Mak, C. L.; Dai, J.; Li, K.; Ye, H.; Leung, C. W., ITO/Au/ITO Sandwich Structure for near-Infrared Plasmonics. *ACS Appl Mater Interfaces* **2014,** *6* (18), 15743-52.
15. Korobkin, D.; Neuner, B.; Fietz, C.; Jegenyes, N.; Ferro, G.; Shvets, G., Measurements of the Negative Refractive Index of Sub-Diffraction Waves Propagating in an Indefinite Permittivity Medium. *Opt. Express* **2010,** *18* (22), 22734-22746.
16. Dao, V. A.; Choi, H.; Heo, J.; Park, H.; Yoon, K.; Lee, Y.; Kim, Y.; Lakshminarayan, N.; Yi, J., Rf-Magnetron Sputtered ITO Thin Films for Improved Heterojunction Solar Cell Applications. *Current Applied Physics* **2010,** *10* (3), S506-S509.

17. Sun, H.; Yu, M.; Wang, G.; Sun, X.; Lian, J., Temperature-Dependent Morphology Evolution and Surface Plasmon Absorption of Ultrathin Gold Island Films. *The Journal of Physical Chemistry C* **2012,** *116* (16), 9000-9008.
18. Krishnamurthy, S.; Esterle, A.; Sharma, N. C.; Sahi, S. V., Yucca-Derived Synthesis of Gold Nanomaterial and Their Catalytic Potential. *Nanoscale Research Letters* **2014,** *9* (1), 627.
19. Han, H.; Theodore, N. D.; Alford, T. L., Improved Conductivity and Mechanism of Carrier Transport in Zinc Oxide with Embedded Silver Layer. *Journal of Applied Physics* **2008,** *103* (1).
20. Chen, C.; Wang, Z.; Wu, K.; Chong, H.; Xu, Z.; Ye, H., ITO–TiN–ITO Sandwiches for near-Infrared Plasmonic Materials. *ACS Applied Materials & Interfaces* **2018,** *10* (17), 14886-14893.
21. Kim, H.; Gilmore, C. M.; Piqué, A.; Horwitz, J. S.; Mattoussi, H.; Murata, H.; Kafafi, Z. H.; Chrisey, D. B., Electrical, Optical, and Structural Properties of Indium–Tin–Oxide Thin Films for Organic Light-Emitting Devices. *Journal of Applied Physics* **1999,** *86* (11), 6451-6461.
22. Naik, G. V.; Shalaev, V. M.; Boltasseva, A., Alternative Plasmonic Materials: Beyond Gold and Silver. *Adv Mater* **2013,** *25* (24), 3264-94.
23. Xu, F.; Mak, C. L.; Shiyu, Z.; Zhewei, W.; Wenjia, Y.; Hui, Y., Pulsed Laser Deposited Indium Tin Oxides as Alternatives to Noble Metals in the near-Infrared Region. *Journal of Physics: Condensed Matter* **2016,** *28* (22), 224009.
24. Wang, Z.; Chen, C.; Wu, K.; Chong, H.; Ye, H., Transparent Conductive Oxides and Their Applications in near Infrared Plasmonics. *physica status solidi (a)* **2019,** *216* (5), 1700794.
25. Mei-Zhen, G.; R, J.; De-Sheng, X.; R, F. W., Thickness Dependence of Resistivity and Optical Reflectance of ITO Films. *CHIN.PHYS.LETT.* **2008,** *25* (4).
26. Benoy, M. D.; Mohammed, E. M.; M., S. B.; P.J., B.; Pradeep, B., Thickness Dependence of Resistivity and Optical Reflectance of ITO Films Prepared by Activated Reactive Evaporation. *Brazilian Journal of Physics* **2009,** *39* (4).
27. Poddubny, A.; Iorsh, I.; Belov, P.; Kivshar, Y., Hyperbolic Metamaterials. *Nature Photonics* **2013,** *7* (12), 948-957.
28. Agranovich, V. M.; Kravtsov, V. E., Notes on Crystal Optics of Superlattices. *Solid State Communications* **1985,** *55* (1), 85-90.
29. Williams, B. L.; Ponomarev, M. V.; Verheijen, M. A.; Knoops, H. C. M.; Chandramohan, A.; Duval, L.; van de Sanden, M. C. M.; Creatore, M., Expanding Thermal Plasma Deposition of Al-Doped ZnO: On the Effect of the Plasma Chemistry on Film Growth Mechanisms. *Plasma Processes and Polymers* **2016,** *13* (1), 54-69.
30. Naik, G. V.; Shalaev, V. M.; Boltasseva, A., Alternative Plasmonic Materials: Beyond Gold and Silver. *Advanced Materials* **2013,** *25* (24), 3264-3294.
31. Calzolari, A.; Ruini, A.; Catellani, A., Transparent Conductive Oxides as near-IR Plasmonic Materials: The Case of Al-Doped ZnO Derivatives. *ACS Photonics* **2014,** *1* (8), 703-709.

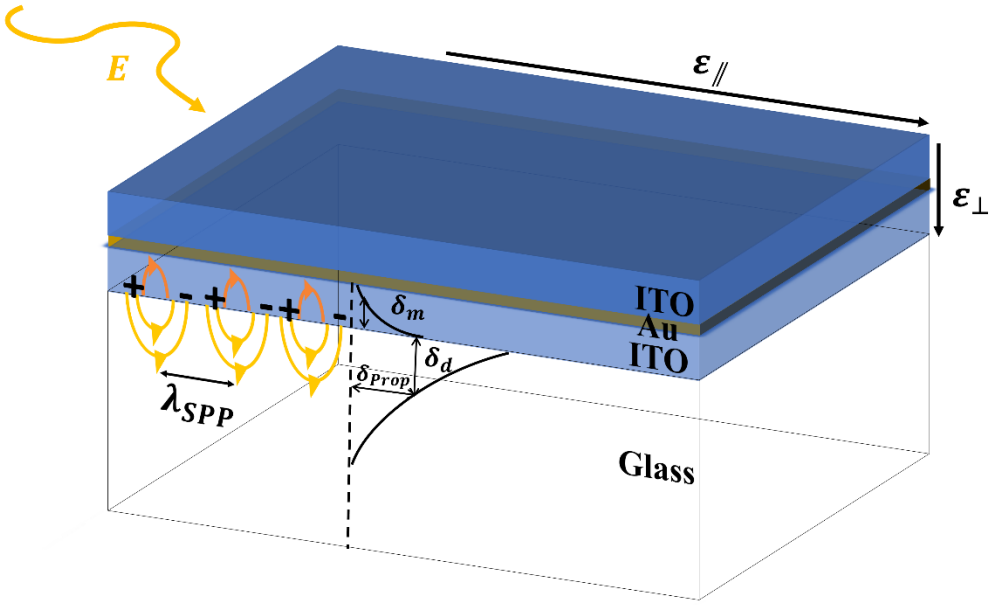

For Table of Contents Only